Materials Research Bulletin 183 (2025) 113220

Contents lists available at ScienceDirect

Materials Research Bulletin

journal homepage: www.elsevier.com/locate/matresbu

Research Papers

Impact of surface oxidation on gilbert damping and inverse spin hall effect in SiO_2/Ta/NiFe multilayers

Pranita Sharma [a], Seunghyun Lee [b], Jonghyeon Choi [b], Jung-Woo Yoo [b], Krishna Begari [a,*], CheolGi Kim [a,*]

[a] Department of Physics and Chemistry, DGIST, Daegu, South Korea
[b] Department of Materials Science and Engineering, UNIST, Ulsan, South Korea

ARTICLE INFO

Keywords:
Spin pumping
Anti-damping
Non-equilibrium spin accumulation
Spin-to-charge conversion
Inverse spin hall effect
Magnetization dynamics

ABSTRACT

Spin pumping in bilayer systems composed of ferromagnetic materials (FM) and heavy metals (HM) generates spin currents that can be detected by the inverse spin Hall effect (ISHE). Here, the reduction in Gilbert's damping (α) during spin pumping and the ISHE in the SiO_2/Ta (tnm)/NiFe (10nm) bilayer system was observed. The value of α for SiO_2/NiFe (10 nm) was determined to be 0.0121 ± 0.0003. However, for SiO_2/Ta (t nm)/NiFe (10 nm), a consistently lower damping across all Ta thicknesses was observed, which could be due to non-equilibrium spin accumulation at the interface. Additionally, high interfacial spin mixing conductance values of -1.83(±0.05) × 10^{19} m^{-2} and a spin diffusion length (λ_{SD}) of 2.77±0.53 nm was obtained. Further high inverse spin Hall voltage was recorded and the spin Hall angle of -0.024 was calculated for the Ta 7 nm system.

1. Introduction

Spintronics devices have gained popularity due to their low power consumption and high speed, making them ideal for next-generation memory and sensing applications [1–4]. Pure spin current (*Js*) generation and detection without charge current have attracted significant attention for meeting these requirements. To utilize pure spin current in modern technology, which mostly uses charge current, the conversion of spin current to charge current is essential. The spin-charge interconversion can be achieved in nonmagnetic (NM) with high spin-orbit coupling (SOC) using the spin Hall effect (SHE) or the inverse spin Hall effect (ISHE) [1]. The conversion efficiency, typically characterized by the spin Hall angle (θ_{SHA}), is thus one of the key parameters for spintronics applications. The spin to charge conversion relation is given by:

$$\overrightarrow{J_c} = \left(\frac{2e}{\hbar}\right)\theta_{SH}\overrightarrow{J_s} \times \overrightarrow{\sigma}$$

Where $\overrightarrow{\sigma}$ is the spin-polarization direction of $\overrightarrow{Js}$. Heavy metals like Pt, Ta, and W, have high spin-orbit interaction (SOC) and low spin-diffusion length which makes them a promising candidate for spin-charge conversion via Inverse Spin Hall effect [1,2,5–9].

Spin pumping, which involves bilayer films consisting of ferromagnetic (FM) materials and nonmagnetic (NM) with high SOC, has emerged as an essential tool for generating spin current (spin accumulation) [1,2,5–7,9–11]. During resonance, the pure spin current from FM layer is transferred to the HM, creating a spin torque. This torque can be measured by spin orbit torque (SOT) efficiency, represented as:

$$\xi_{SH} = \left(\frac{2e}{\hbar}\right)\frac{J_s}{J_c}$$

The efficiency of this spin angular momentum transfer is governed by magnetization precession; therefore, Gilbert Damping and saturation magnetization play crucial roles in an efficient spin pumping mechanism. The impact of spin pumping on the Gilbert damping values of different FM/NM have been extensively studied in the last decade [1,2,6–8,12–19].

In most cases, the damping constant is generally enhanced due to spin pumping [2,12,20]. However, for low-power applications, a lower damping constant is preferred. To accomplish this, direct current (DC) can be applied to the nonmagnetic layer, which induces an opposite torque through Rashba interaction [21–24]. In the presence of a DC magnetic field, the non-equilibrium spin density builds up at the interface of the ferromagnetic (FM) and non-magnetic (NM) materials due to the structural inversion asymmetry. This accumulated spin density

* Corresponding authors.
E-mail addresses: krishnabegari.phy@gmail.com (K. Begari), cgkim@dgist.ac.kr (C. Kim).

https://doi.org/10.1016/j.materresbull.2024.113220
Received 13 August 2024; Received in revised form 5 November 2024; Accepted 18 November 2024
Available online 22 November 2024

interacts with the magnetization of the FM layer through ferromagnetic exchange coupling. As a result, magnetization can be reversed at high current densities, a phenomenon known as the anti-damping of magnetization precession. This process effectively reduces the Gilbert damping constant (α) compared to a bare FM. However, it also diminishes the device's operational efficiency.

Recently, non-equilibrium spin accumulation has been also observed during the process of spin pumping at the interface in the FM/NM system [25]. It becomes more prominent when the heavy metal thickness is smaller or comparable to its spin diffusion length. In this thickness regime, the non-equilibrium spin accumulation stimulates an extra torque on the FM spins, which results in the decrease of the damping parameter even in absence of external DC involvement. Thus, the spin pumping mechanism offers a direct approach to effectively utilize the interfacial Rashba effect thereby reducing the critical current requirement without degrading the device efficiency [6,7,13,25].

In this study, reduced damping in SiO_2/Ta (tnm)/NiFe (10nm) as compared to the Single layer SiO_2/NiFe was analyzed by ferromagnetic resonance (FMR) measurements. This anti-damping in the bilayer caused by Rashba-like SOT was obtained without external DC field. Although this observation is similar to the anti-damping effect observed in β-Ta/Py/SiO_2/Si(100) [6], it rules out the possibility of protecting the underlying NiFe layer due to Ta layer. Further high interfacial spin mixing conductance and spin current density were calculated. At resonance, the spin current transferred from NiFe into the Ta layer is converted into a charge current through the inverse spin Hall effect (ISHE). Further, the spin Hall angle of SiO_2/Ta (7nm)/NiFe (10nm) sample can be estimated by measuring the voltage across the sample.

This study underscores the potential of Ta as a material for inducing Rashba-like torque leading to lower α. This characteristic of Ta could be instrumental in developing low power spintronics devices due to the absence of any DC-current [6].

2. Experiment techniques

SiO_2/NiFe (10nm) and SiO_2/Ta (tnm)/NiFe (10nm) samples were deposited on 5 mm x 5 mm SiO_2/Si substrates using DC magnetron sputtering. $Ni_{80}Fe_{20}$ and Ta were deposited on the same chamber at 4.5 mTorr argon pressure and 50 mA current. The base pressure was around 1×10^{-7}Torr, and deposition pressure was maintained at 4.3×10^{-3} Torr. Before deposition, the substrates were thoroughly cleaned with Alconox, acetone, methanol, and deionized water in an ultrasonic water bath and the targets were pre-sputtered for 10 min. The Ta layer thickness ranges as 0, 1, 3, 5, 7, 9, 11 and 13 nm. The thickness of the samples was calculated using the premeasured deposition rate obtained through X-ray reflectivity (XRR).

Crystallographic properties of films were determined using X-ray diffraction (XRD) technique using a Panalytical/Empyrean diffractometer with Cu-Kα radiation (λ = 1.5406 Å) as the radiation source. Diffraction patterns of Ta samples with thickness 10 nm, 20 nm and 30 nm were recorded using Grazing Incident angle mode at omega equal to 0.5° to find the Ta phase in our samples. Sheet resistance of Ta (tnm) and NiFe were measured using a four-probe method.

Magnetization dynamics were studied using a ferromagnetic resonance (FMR) technique for excitation frequencies of 9–19 GHz at room temperature. A DC magnetic field (H), perpendicular to the radio frequency field (h_{rf}), was applied using an electromagnet. The HM/NM bilayer was placed between the ground (G) and signal (S) lines of a coplanar waveguide as shown in Fig. 1(a,b) [10].

Additionally, X-ray photoelectron spectroscopy (XPS, Thermo Fisher Escalab 250Xi) using Al-K_α(1486.61 eV) as a radiation source was utilized for studying the depth profile of the samples.

To measure ISHE voltage a nanovoltmeter was connected to the FMR set-up to measure voltage transverse to the applied field. A 5×2 mm^2 Ta-Au contact was deposited over the sample using a shadow mask for connections.

3. Results and discussion

Fig. 2(a) shows the XRD patterns of single layer Ta thin film of thickness 10 nm, 20 nm and 30 nm obtained using glancing angle of incidence of 0.5° Due to low thickness, the observation of significant peaks for thickness below 10 nm was not noticed. A broad peak at 38° can be seen for 30 nm which gradually shifts to 37.2° for 10 nm. It is difficult to distinguish if the XRD peak is of α-(110) or β-(202) as the spectrum is quite broad and the calculated d-spacing of 0.23 $\AA$ is common for both phases. Given that the 2θ value is much lower than that of α-(110) which occurs at 38.47°, especially for 10 nm, this peak can assigned to (202) lattice planes of the tetragonal β-Ta crystal (JCPDS 25–1280) [26]. The absence of the isolated α-Ta (200) peak at 56.0° and presence of the peak at 67° corresponding to *(004)* peak of β-Ta further confirms the presence of β-Ta [26].

In addition to XRD, resistivity measurement was conduction to support the β-Ta formation. The resistivity was estimated using the four-probe method by fitting the measured sheet resistance of different Ta thickness (Fig.:2(b)) using the equation:

$$R = \frac{\rho_{Ta}}{t_{Ta}} + C\ \Omega$$

The resistivity(ρ_{Ta}) value of ~317.34 (±12.0) $\mu\Omega{\cdot}cm$ extracted from the above equation is in good agreement with the published results [27,28], which additionally confirms the desired β-phase Ta thin films growth rather than the α-phase of lower resistivity (15–60 $\mu\Omega{\cdot}$cm) [1,29,30]. Even though there is a sharp decrease in the resistivity with thickness, the values for thicker films used in this work still falls in the range for resistivity of β-Ta. The resistivity of NiFe (10 nm) ~ 77.49 $\mu\Omega{\cdot}$cm was directly calculated from sheet resistance using four-probe.

The FMR spectra of the SiO_2/NiFe (10nm), and SiO_2/Ta (t_{Ta})/NiFe (10nm) were acquired across a frequency (f) range of 9–19 GHz with measurements taken every 2 GHz, using a microwave power of 30 dBm.

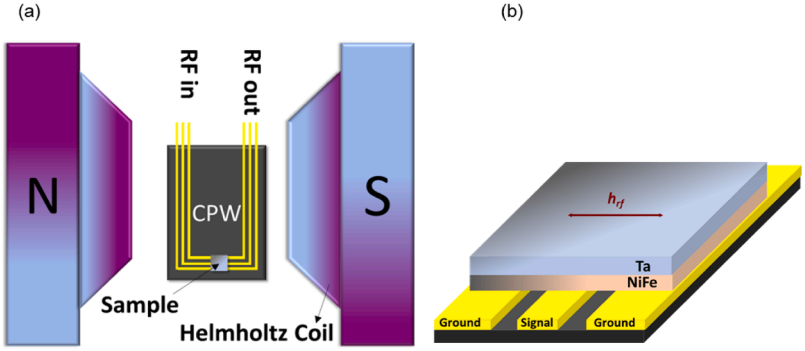

Fig. 1. (a,b) Ferromagnetic Resonance Measurement using Co-planner Waveguide.

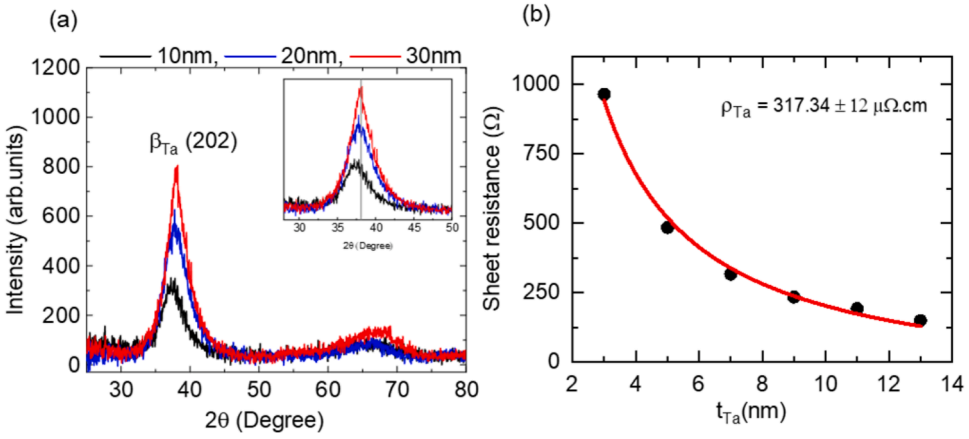

Fig. 2. (a) X-ray diffraction of Ta and (b) Resistance as a function of Ta thickness.

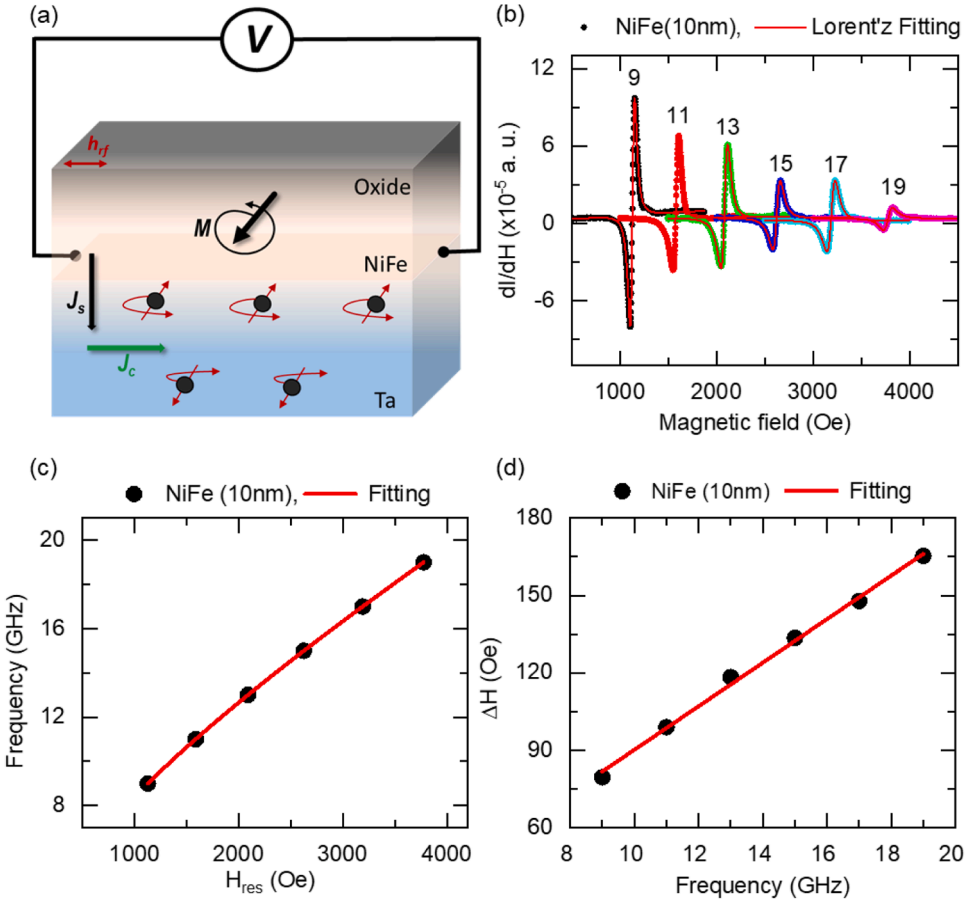

Fig. 3. (a) FMR- ISHE mechanism and voltage measurement schematics, (b) FMR spectra of single layer NiFe sample, (c) frequency versus *Hres* and (d) *ΔH* versus frequency.

Fig. 3(a) shows the mechanism of the FMR-ISHE measurement. For determining the resonance field H_{res} and linewidth ΔH at different frequencies, the observed FMR spectra were fitted with the derivative of the Lorentzian function given by equation (1) [2,6]

$$\frac{dI}{dH} = k_1 \frac{4\Delta H(H - H_{res})}{\left(\Delta H^2 + 4(H - H_{res})^2\right)^2} + k_2 \frac{\Delta H^2 - 4(H - H_{res})^2}{\left(\Delta H^2 + 4(H - H_{res})^2\right)^2} \quad (1)$$

FMR spectra of single layer NiFe sample, frequency versus H_{res} and ΔH versus frequency is shown in Fig. 3 (b, c & d), respectively.

The saturation magnetization (M_S) of the samples can be calculated by fitting the frequency vs H_{res} plot to the Kittel equation [2,6,15]:

$$f_r = \frac{\gamma}{2\pi}\sqrt{(H_{res} + H_k)(H_{res} + H_k + 4\pi M_s)} \quad (2)$$

Here, H_k is the uniaxial anisotropy, and γ is the gyromagnetic ratio. The values of the saturation magnetization $4\pi M_S$ of 7852.11 Oe were extracted for a single layer NiFe sample.

Gilbert's damping parameter (α) of 0.0121 ± 0.0003 was estimated for NiFe film by fitting the frequency versus linewidth (ΔH) plot using the following relation [2,6]:

$$\Delta H = \Delta H_o + \frac{4\pi\alpha f}{\gamma} \quad (3)$$

Here, ΔH_o is the line broadening due to extrinsic contributions. This value of $4\pi M_S$ and α for single-layer NiFe film is comparable to the previous reports [14,31].

In case of the bilayer layer system, due to spin accumulation the FMR conditions and therefore values of M_S and α are manipulated. Frequency versus *Hres* plot and the extracted values of M_S for different Ta thicknesses are presented in Fig. 4(a & b). The M_S values for the bilayer system ranges from 7914.43 Oe to 9638.85 Oe and within estimation error, these $4\pi M_S$ values for the bilayers are clearly larger than that of the single layer NiFe layer. This enhancement in $4\pi M_S$, could be due to extra spin density from spin accumulation in the heavy metal layer, which is theoretically linked to the strong local spin-orbit coupling at the interface because of magnetic proximity effect in NiFe due to the adjacent Ta layer [6,13]. VSM measurement was performed to verify the effect, Figure S1 shows the M_S values measured in VSM for Bilayer are more than that of Single Layer NiFe which confirms the existence of proximity effect observed in FMR measurement [32–34].

Linewidth (ΔH) vs Frequency plot for NiFe and bilayer samples with varying Ta thickness is plotted in Fig. 4(c). As the relation is linear, we can estimate the damping paraments of individual samples from the slope of the line. It can be observed that the slope of the line is lower for bilayer samples showing narrowing of the linewidth compared to the single-layer NiFe. Narrowing of the linewidth indicates a decrease in the whole relaxation of the magnetization dynamics. The reduction in the Gilbert damping coefficient calculated using Eq. (3) for the SiO_2/Ta (tnm)/NiFe (10nm) bilayer sample confirms that the reduction in linewidth is due to a decrease in the relaxation processes that characterize the magnetic system [35].

The observed enhancement in $4\pi M_S$, together with the relaxation of magnetization dynamics observed in FMR, supports the presence of a strong spin-orbit torque (SOT) leading to anti-damping. The observed anti-damping can be due to the back flow of spin current into the NiFe layer or spin accumulation at the interface which generates an additional SOT on the in-plane magnetization of the NiFe layer. This spin accumulation is highly influenced on spin diffusion length λ_{SD} of the Ta layer. Fig. 4(d) shows the relation of α_{eff} with Ta thickness, where $\alpha_{eff} = (\alpha_{Ta/Py} - \alpha_{Py})$ is the difference between the damping constant of bilayer and single layer system samples. A sharp decrease in α_{eff} till 5 nm was observed after which it was almost constant, which is very similar to the results reported by Panigrahi but contrasting to Behera where after a certain thickness around 2-times spin depth, the alpha effect increased. In either case, the effective damping was negative for all thicknesses of Ta.

According to the theoretical model for α_{eff} versus t_{Ta} proposed by Tserkovnyak et al. [16,17],the pure spin current J_S injected from the FM layer accumulates at the interface of the NM layer resulting in the non-equilibrium spin density causing a backflow of spin angular momentum to the FM layer, which opposes the enhancement of α_{eff}. Similar anti-damping behavior was reported in NiFe/ β-Ta bilayer samples by Behera et al. [6] and CoFe/Ta structure studied by Panigrahi et al. [36]. The reduction in damping value for SiO_2/Ta (tnm)/NiFe (10nm) can be linked to Inverse Rashba spin-orbit interaction at the interface due to non-equilibrium spin accumulation at the interface [7,36].

The values of spin diffusion length (λ_{SD}) and $Re(g^{eff}_{\uparrow\downarrow})$; the real part of interfacial effective spin mixing conductance of the system can be extracted from the Eq. (4) [12,16].

$$\alpha_{eff} = \frac{g\mu_B Re(g^{eff}_{\uparrow\downarrow})}{4\pi M_s t_{FM}} \left(1 - e^{-\frac{2t_{Ta}}{\lambda_{sd}}}\right) \quad (4)$$

where $g = 2.1$, $\mu_B = 9\ 274 \times 10^{-21}$ ergs/Oe is the Bohr magneton. A higher value of $g^{eff}_{\uparrow\downarrow}$ is indicative of a stronger spin current in the NM layer. For our system, $\lambda_{SD} \sim 2.77 \pm 0.53$ nm and $g^{eff}_{\uparrow\downarrow}$ was calculated to be

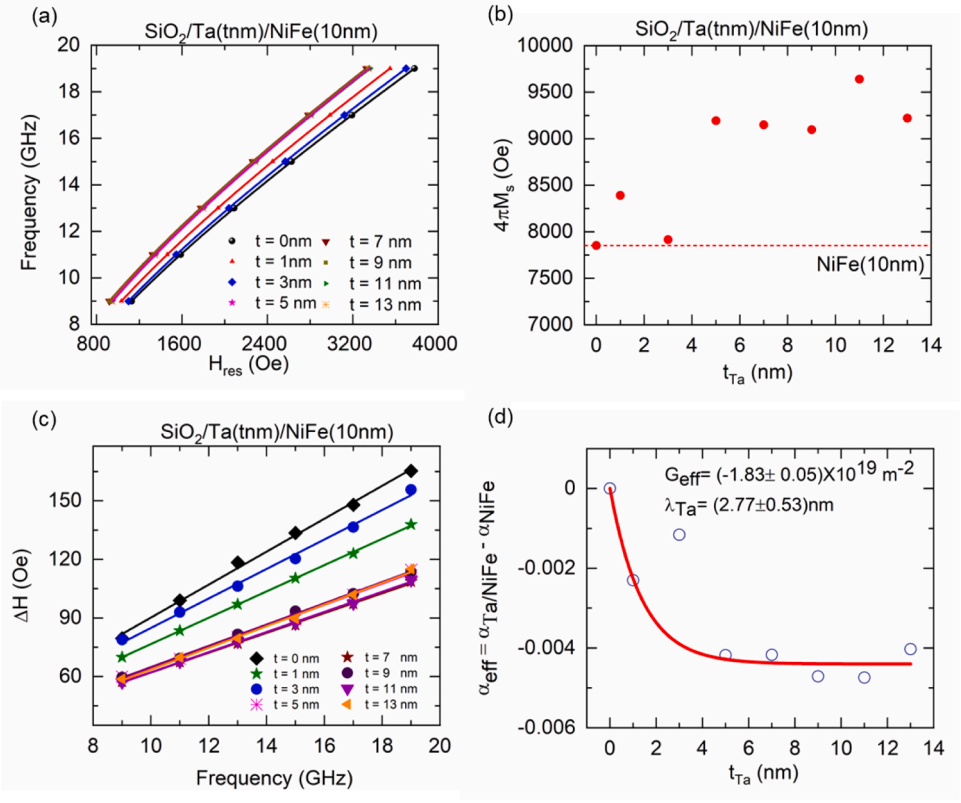

Fig. 4. (a) Frequency vs *Hres*, (b) Saturation magnetization (c) ΔH vs Frequency and (d) Effective damping constant, for different Ta thickness.

-1.83 (± 0.05) $E + 19$ m^{-2}. The negative sign indicates a net flow of angular momentum into the ferromagnetic layer and is a characteristic of anti-damping [30]. The effective spin mixing conductance ($g_{\uparrow\downarrow}^{eff}$) characterizes the efficiency of spin transport across interfaces in magnetic multilayer systems and therefore considers both the initial spin pumping and the inward and outward back flow(net flow) [1]. These values are higher than many previous reports and comparable to CoFeAl/beta-Ta films studied by Serkan Akansel et al. [12].

Since the sample does not have a capping layer, the NiFe layer might have oxide formation at the surface. The presence of oxide introduces structural inversion asymmetry in the NiFe, leading to non-equilibrium spin accumulation and an inverse Rashba-like spin-orbit interaction in the system [13]. The XPS depth profile measurements were conducted to support the proposed explanation for the decrease in effective damping behavior. The variation in the XPS signal of Ni-2p, Fe-2p and O-1 s for single layer NiFe is shown in Fig. 5(a, b, and c) Ni-2p and Fe-2p spectrum has 3 significant peaks located at 852.5, 854.8, and 860.8 eV, which corresponds to the metallic Ni, NiO, and satellite phases and 706.4, 711.7 and 721.8 eV corresponding to metallic Fe, Fe_2O_3 and satellite peak respectively. The XPS spectra of O-1 s can be deconvoluted into three peaks at 529.4, 531.1, and 532.75 eV The 529.4 eV peak can be ascribed to lattice oxygen in polycrystalline NiO, further confirming the existence of NiO.

The peak features positioned at 530.5 and 531.3 eV can be attributed to oxide and hydroxy groups of the NiFe alloy, respectively [37–40]. Fig. 5d shows XPS spectra of Ta-4f obtained after 90 s etch time. Two prominent metallic peaks at 21.65 eV and 23.45 eV and corresponding satellite peaks were observed [41–43].

From the XPS spectra, the formation of a thin oxide layer at the surface is confirmed, which could facilitate Rashba like interaction in the system [13,44]. Further, the consistency and independence of the oxide layer thickness, regardless of the underlying Ta layer thickness, support the observation that the reduction in damping occurs irrespective of the Ta layer thickness. Similar behavior was reported by many groups for thin Ta and Al capped layers for both current driven as well as spin pumped systems [13,44].

Under ferromagnetic resonance conditions, the accumulated spin current in the Ta layer is converted into charge current through the Inverse Spin Hall Effect, as depicted in Fig. 3(a). Voltage measurements were carried out for Ta (tnm)/NiFe (10nm) at all frequency ranges used for FMR measurement. The FMR spectra and its corresponding voltage measured for Ta (7nm)/NiFe (10nm) sample at 9 GHz frequency is shown in Fig 6(b & c) in order. It is observed that the voltage peak and the zero-crossing point of the derivative FMR spectrum coincide at the same resonance field. This phenomenon suggests the occurrence of spin pumping-induced Inverse Spin Hall Effect (ISHE). The voltage signal $V(H)$ consists of symmetric and asymmetric components that can be represented by a Lorentzian expression, given by [7,8],

$$V(H) = \frac{V_{sym}\Delta H^2}{\Delta H^2 + (H - H_{res})^2} + \frac{V_{asym}(H)\Delta H(H - H_{res})}{\Delta H^2 + (H - H_{res})^2} \quad (5)$$

Where V_{sym} and V_{asym} refer to the symmetric and asymmetric component of the measured voltage. The symmetric part represents the contribution from ISHE, and the asymmetric part represents the contributions from other spin rectification effects [2,18].

The fitting indicates that the significant contribution to the voltage is primarily from the symmetric component. To rule out the possibility of other contributions in the symmetric voltage, voltage was measured by changing the polarity of magnetic field. The reversal of the external magnetic field causes a sign change in the polarization of the pumped spin current and thus leads to a change of the sign of the spin pumping

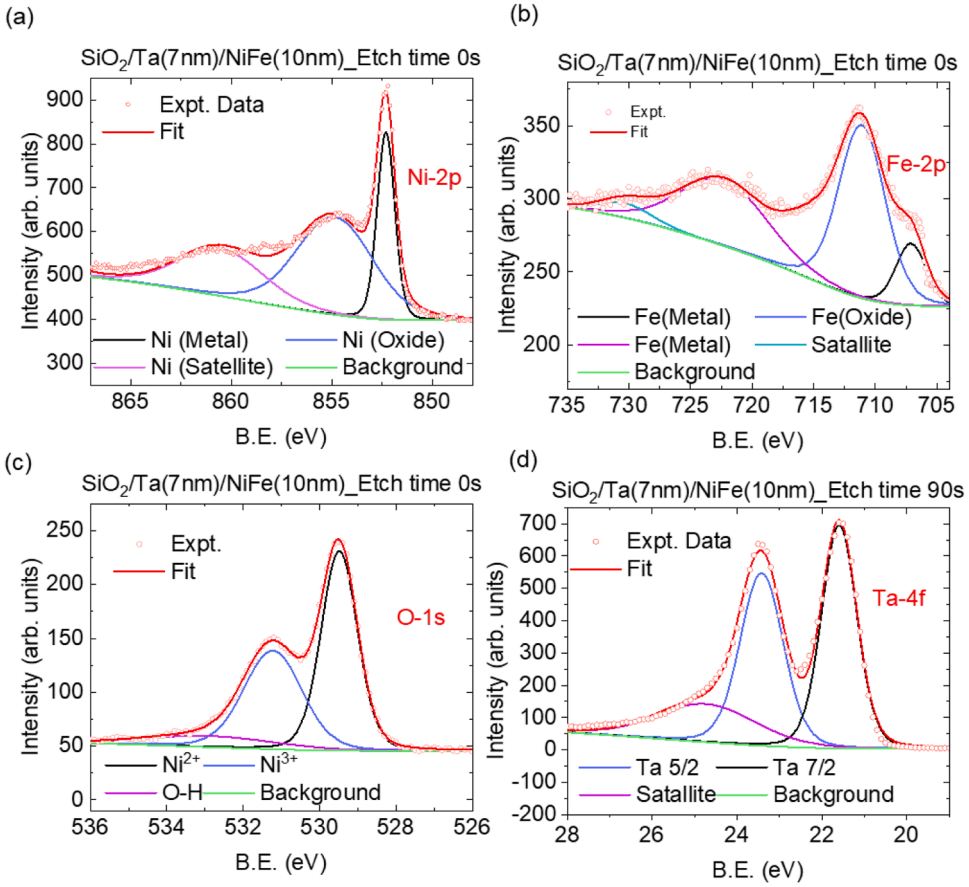

Fig. 5. XPS spectra of SiO2/Ta (7nm)/NiFe (10nm) corresponding to (a) Ni-2p (b) Fe-2p (c) O-1 s and (d)Ta-4f.

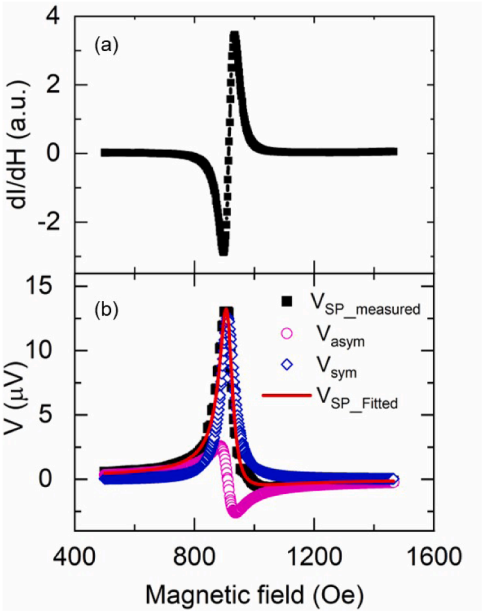

Fig. 6. (a) FMR spectra and (b) corresponding voltage measured for Ta (7nm)/NiFe (10nm) sample at 9 GHz frequency.

voltage. Fig. 7(a) depicts the measured voltage signal of Ta (7nm)/NiFe (10nm) sample for both negative and positive applied field. The polarity of the symmetric voltage changes which is a signature of ISHE while the asymmetric part remains the same, and the magnitude of Voltage is comparable for both polarities which indicates that the voltage is from ISHE as predicted theoretically [45–47].

Fig. 7(b) shows voltage for a wide range of excitation frequencies (9–19 GHz) with a field sweep from ±4000 Oe The ISHE peak shift is consistent with FMR resonant modes for NiFe [8]. Further, Ta thickness-dependent voltage measurement was conducted to see the dependence of voltage due to ISHE as a function of Ta thickness (Fig 8(a & b)). The Voltage initially increases till around 6 nm and then gradually decreases. This is again significant ISHE behavior as the effect is prominent till tnm $< 2\lambda_{sd}$.

To quantify the efficiency of this spin-to-charge conversion, the intensity of the spin can be calculated from the vertical spin current density, J_S written as [8,15]

$$J_S = \frac{G_{\uparrow\downarrow}\gamma^2\hbar h_{rf}^2}{8\pi\alpha^2_{(Ta/NiFe)}}\left[\frac{4\pi M_s\gamma + \sqrt{(4\pi M_s\gamma)^2 + 4\omega^2}}{(4\pi M_s\gamma)^2 + 4\omega^2}\right]\frac{2e}{\hbar} \quad (6)$$

where h_{rf} is the rf magnetic field which is 0.84 Oe for our setup, The factor $\frac{2e}{\hbar}$ in Eq. (6) converts the unit of spin current from J/m^2 to A/m^2, which is equivalent to a three-dimensional current density [15]

The spin current density described in Eq. (6) is converted into an electromotive force V_{ISHE} due to the ISHE in the Ta layer induced by the spin pumping as per the following relation:

$$\frac{V_{ISHE}}{w} = \frac{j_s\theta_{SH}\lambda_{SD}\tanh\left(\frac{t_N}{2\lambda_{SD}}\right)}{\sigma_{NiFe}t_{FNiFe} + \sigma_{Ta}t_{Ta}} \quad (7)$$

where ρ_{NiFe} and ρ_{Ta} are the resistivities of the NiFe and Ta thin films, respectively. The parameters $w = 0.42$ mm, t_{NiFe}, t_{Ta} are the width of the signal line of cpw, and the thickness of the NiFe and Ta layer, respectively [7,8,13].

Using Eq. (7) the value of $|J_S|$ and θ_{SHA} for Ta (7nm)/NiFe (10nm) sample was calculated to be 7825.635 MA/m^2 and −0.024, respectively.

4. Conclusion

FMR-ISHE measurements of SiO_2/Ta (tnm)/NiFe (10nm) sample revealed a lower Gilbert damping parameter of 0.008 for the SiO2/Ta (tnm)/NiFe (10 nm) sample, compared to a parameter of 0.012 observed in the bare NiFe sample. This reduction in damping is notable since an increase in the effective damping constant (α_{eff}) was anticipated due to spin pumping effects. The observed trend in Gilbert damping, particularly in the absence of an external DC applied to the non-magnetic (NM) layer, could be due to oxidation at the surface of NiFe leading to a structural inversion asymmetry on the Py layer, resulting in non-equilibrium spin accumulation and an Inverse Rashba-like spin-orbit interaction within the system.

Additionally, high interfacial spin mixing conductance values of $-1.83\ (\pm 0.05) \times 10^{19}$ m^{-2} and a spin diffusion length (λ_{SD}) of 2.77±0.53 nm was extracted from thickness dependent effective damping; $\alpha_{eff} = (\alpha_{Ta/Py} - \alpha_{Py})$ relation. The transverse voltage recorded during spin pumping had a polarity-dependent high symmetric Lorentzian contribution showing dominance of the inverse spin Hall effect over other spin rectification effects. The V_{ISHE} increases with Ta thickness till ~7 nm ($2\lambda_{SD}$) after which it decreases. From the voltage measurements, spin current density $|J_S|$ of 7825.635 MA/m^2 and spin hall angle θ_{SHA} of −0.024 was calculated for the SiO_2/Ta (7nm)/NiFe (10nm) sample.

The tunability of effective damping constant along with ISHE highlights the prospective application of the SiO_2/Ta/NiFe system for the development of low power spintronics devices for various memory and sensing applications.

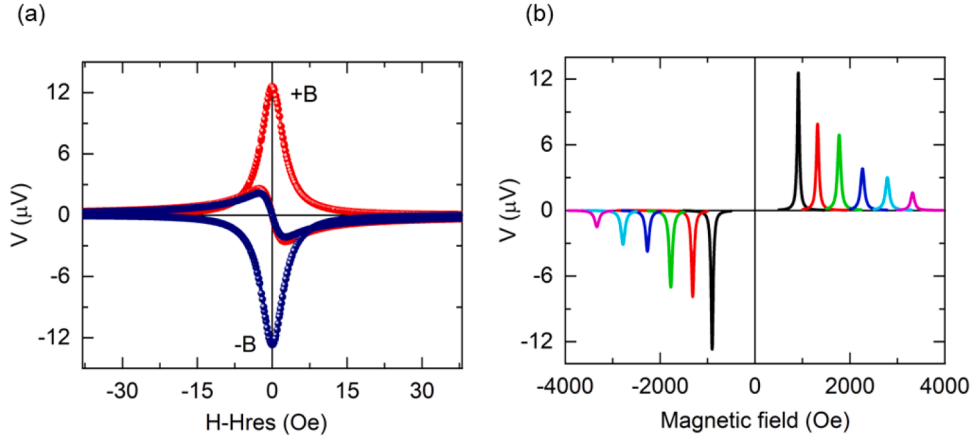

Fig. 7. (a) The DC voltage measured for Ta(7nm)/NiFe(10) sample when negative and positive field is applied and (b) Voltage measured at different excitation frequencies (9–19 GHz).

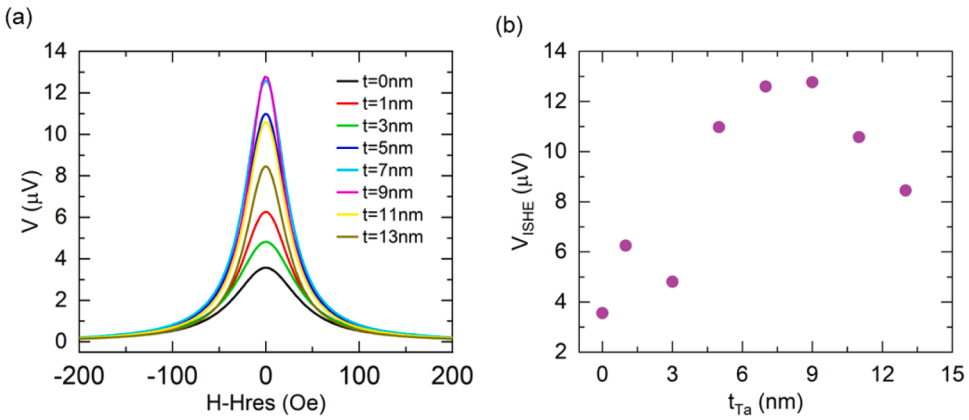

Fig. 8. Inverse spin hall effect (a) voltage signal and (b) V_{ISHE} in the function of Ta thickness.

CRediT authorship contribution statement

Pranita Sharma: Writing – original draft, Investigation, Formal analysis, Data curation, Conceptualization. **Seunghyun Lee:** Software, Data curation. **Jonghyeon Choi:** Software, Data curation. **Jung-Woo Yoo:** Resources. **Krishna Begari:** Writing – review & editing, Supervision, Formal analysis. **CheolGi Kim:** Writing – review & editing, Supervision, Resources, Funding acquisition.

Declaration of competing interest

The authors declare that they have no known competing financial interests or personal relationships that could have appeared to influence the work reported in this paper.

Acknowledgement

The authors acknowledge funding from the National Research Foundation of Korea (NRF) grant funded by the Korean government (MSIT) (Grant No. NRF-2018R1A5A1025511) and in part by the R&D program of MOTIE (Grant No. 00236809).

Supplementary materials

Supplementary material associated with this article can be found, in the online version, at doi:10.1016/j.materresbull.2024.113220.

Data availability

Data will be made available on request.

References

[1] R. Yu, B. Miao, L. Sun, Q. Liu, J. Du, P. Omelchenko, B. Heinrich, M. Wu, H. Ding, Determination of spin Hall angle and spin diffusion length in β-phase-dominated tantalum, Phys. Rev. Mater. 2 (7) (2018) 074406.
[2] K. Ando, S. Takahashi, J. Ieda, Y. Kajiwara, H. Nakayama, T. Yoshino, K. Harii, Y. Fujikawa, M. Matsuo, S. Maekawa, Inverse spin-Hall effect induced by spin pumping in metallic system, J. Appl. Phys. 109 (10) (2011) 103913.
[3] B. Behin-Aein, D. Datta, S. Salahuddin, S. Datta, Proposal for an all-spin logic device with built-in memory, Nat. Nanotechnol. 5 (4) (2010) 266–270.
[4] Y. Xu, Y. Yang, M. Zhang, Z. Luo, Y. Wu, Ultrathin All-in-One Spin Hall Magnetic Sensor with Built-In AC Excitation Enabled by Spin Current, Adv. Mater. Technol. 3 (8) (2018) 1800073.
[5] J.E. Gomez, B.Z. Tedlla, N.R. Alvarez, G. Alejandro, E. Goovaerts, A. Butera, Spin transport parameters in ni 80 fe 20/ru and ni 80 fe 20/ta bilayers, Phys. Rev. B 90 (18) (2014) 184401.
[6] N. Behera, S. Chaudhary, D.K. Pandya, Anomalous anti-damping in sputtered β-Ta/Py bilayer system, Sci. Rep. 6 (1) (2016) 1–9.
[7] P. Gupta, B.B. Singh, K. Roy, A. Sarkar, M. Waschk, T. Brueckel, S. Bedanta, Simultaneous observation of anti-damping and the inverse spin Hall effect in the La (0.67)Sr(0.33)MnO(3)/Pt bilayer system, Nanoscale 13 (4) (2021) 2714–2719, https://doi.org/10.1039/d0nr06228f.
[8] B. Paikaray, S.K. Sahoo, T. Manoj, K. Sriram, H. Basumatary, A. Haldar, C. Murapaka, Large spin pumping and inverse spin Hall effect in Ta/Py bilayer structures, *physica status solidi* (a) 219 (11) (2022) 2100608.
[9] R. Hao, K. Zhang, W. Chen, J. Qu, S. Kang, X. Zhang, D. Zhu, W. Zhao, Significant role of interfacial spin–orbit coupling in the spin-to-charge conversion in pt/nife heterostructure, ACS. Appl. Mater. Interfaces. 14 (51) (2022) 57321–57327.
[10] J. Park, I. Oh, A.-Y. Lee, H. Jang, J.-W. Yoo, Y. Jo, S.-Y. Park, The effect of graphene interlayer at Pt/YIG interface on spin pumping, J. Alloys. Compd. 829 (2020) 154534.
[11] S.P. Pati, Study on the Gilbert damping of polycrystalline YIG films with different capping layers, Curr. Appl. Phys. 20 (1) (2020) 167–171.
[12] S. Akansel, A. Kumar, N. Behera, S. Husain, R. Brucas, S. Chaudhary, P. Svedlindh, Thickness-dependent enhancement of damping in C o 2 FeAl/β-Ta thin films, Phys. Rev. B 97 (13) (2018) 134421.
[13] N. Behera, P. Guha, D.K. Pandya, S Chaudhary, Capping Layer (CL) Induced Antidamping in CL/Py/Ī²-W System (CL: al, Ī²-Ta, Cu, Ī²-W), ACS. Appl. Mater. Interfaces. (2017).
[14] L. Cai, C. Yu, W. Zhao, Y. Li, H. Feng, H.-A. Zhou, L. Wang, X. Zhang, Y. Zhang, Y. Shi, The Giant Spin-to-Charge Conversion of the Layered Rashba Material BiTeI, Nano Lett. 22 (18) (2022) 7441–7448.
[15] W. Zhang, M.B. Jungfleisch, W. Jiang, J.E. Pearson, A. Hoffmann, Spin pumping and inverse rashba-edelstein effect in NiFe/Ag/Bi and NiFe/Ag/Sb, J. Appl. Phys. 117 (17) (2015) 17C727.
[16] Y. Tserkovnyak, A. Brataas, G.E. Bauer, Enhanced Gilbert damping in thin ferromagnetic films, Phys. Rev. Lett. 88 (11) (2002) 117601.
[17] Y. Tserkovnyak, A. Brataas, G.E. Bauer, Spin pumping and magnetization dynamics in metallic multilayers, Physical Review B 66 (22) (2002) 224403.
[18] W. Zhang, V. Vlaminck, J.E. Pearson, R. Divan, S.D. Bader, A. Hoffmann, Determination of the Pt spin diffusion length by spin-pumping and spin Hall effect, Appl. Phys. Lett. 103 (24) (2013) 242414.
[19] S.P. Pati, Influence on the Gilbert damping of yttrium-iron-garnet films by the spin-pumping effect, Mater. Sci. Semicond. Process. 107 (2020) 104821.
[20] S.P. Pati, Y. Endo, Enhanced low-temperature interfacial gilbert damping in pt/yig/pt trilayer structures, IEEE Trans Magn 55 (2) (2018) 1–4.
[21] L. Liu, C.-F. Pai, Y. Li, H. Tseng, D. Ralph, R. Buhrman, Spin-torque switching with the giant spin Hall effect of tantalum, Science (1979) 336 (6081) (2012) 555–558.
[22] J. Kim, J. Sinha, M. Hayashi, M. Yamanouchi, S. Fukami, T. Suzuki, S. Mitani, H. Ohno, Layer thickness dependence of the current-induced effective field vector in Ta| CoFeB| MgO, Nat. Mater. 12 (3) (2013) 240–245.
[23] A. Manchon, H.C. Koo, J. Nitta, S.M. Frolov, R.A. Duine, New perspectives for Rashba spin–orbit coupling, Nat. Mater. 14 (9) (2015) 871–882.
[24] G. Allen, S. Manipatruni, D.E. Nikonov, M. Doczy, I.A. Young, Experimental demonstration of the coexistence of spin Hall and Rashba effects in β− tantalum/ferromagnet bilayers, Phys. Rev. B 91 (14) (2015) 144412.
[25] F. Liu, C. Zhou, R. Tang, G. Chai, C. Jiang, Controllable charge-spin conversion by Rashba-Edelstein effect at Cu/Ta interface, J. Magn. Magn. Mater. 540 (2021) 168462.
[26] L. Liu, J. Xu, S. Jiang, Nanocrystalline β-Ta Coating Enhances the Longevity and Bioactivity of Medical Titanium Alloys, Metals. (Basel) 6 (9) (2016) 221.
[27] M. Magnuson, G. Greczynski, F. Eriksson, L. Hultman, H. Högberg, Electronic structure of β-Ta films from X-ray photoelectron spectroscopy and first-principles calculations, Appl. Surf. Sci. 470 (2019) 607–612.
[28] M.H. Read, C. Altman, A new structure in tantalum thin films, Appl. Phys. Lett. 7 (3) (1965) 51–52.
[29] E. Montoya, P. Omelchenko, C. Coutts, N.R. Lee-Hone, R. Hübner, D. Broun, B. Heinrich, E. Girt, Spin transport in tantalum studied using magnetic single and double layers, Phys. Rev. B 94 (5) (2016) 054416.
[30] N. Behera, S. Chaudhary, D.K. Pandya, Anomalous anti-damping in sputtered β-Ta/Py bilayer system, Sci. Rep. 6 (1) (2016) 19488.
[31] H. Nakayama, K. Ando, K. Harii, T. Yoshino, R. Takahashi, Y. Kajiwara, K.-i. Uchida, Y. Fujikawa, E Saitoh, Geometry dependence on inverse spin Hall effect induced by spin pumping in Ni 81 Fe 19/Pt films, Phys. Rev. B 85 (14) (2012) 144408.

[32] S.P. Pati, M. Al-Mahdawi, Y. Shiokawa, M. Sahashi, Y. Endo, Effect of a platinum buffer layer on the magnetization dynamics of sputter deposited YIG polycrystalline thin films, IEEE Trans. Magn. 53 (11) (2017) 1–5.
[33] A. Moura, Theoretical analysis of FMR-driven spin pumping current and its properties via the self-consistent harmonic approximation, Phys. Rev. B 106 (5) (2022) 054313.
[34] Y. You, H. Sakimura, T. Harumoto, Y. Nakamura, J. Shi, C. Song, F. Pan, K. Ando, Study of spin mixing conductance of single oriented Pt in Pt/Ni81Fe19 heterostructure by spin pumping, AIP. Adv. 11 (3) (2021).
[35] Hermanny, E.; González-Chávez, D.; Sommer, R. Major effective-damping reduction achieved by metallic coating on YIG thin films. 2021.
[36] B. Panigrahi, S.K. Sahoo, S. S K, J. Sinha, H. Basumatary, M.M. Raja, A Haldar, Effect of Ta capping layer on spin dynamics in Co50Fe50 thin films, Solid. State Commun. (2022) 348–349, https://doi.org/10.1016/j.ssc.2022.114743.
[37] F. Bao, E. Kemppainen, I. Dorbandt, F. Xi, R. Bors, N. Maticiuc, R. Wenisch, R. Bagacki, C. Schary, U. Michalczik, Host, suppressor, and promoter—The roles of Ni and Fe on oxygen evolution reaction activity and stability of NiFe alloy thin films in alkaline media, ACS. Catal. 11 (16) (2021) 10537–10552.
[38] Z. He, Z. Li, X. Jiang, C. Wu, Y. Liu, X. Song, Z. Yu, Y. Wang, Z. Lan, K. Sun, Surface Investigation of Ni81Fe19 Thin Film: using ARXPS for Thickness Estimation of Oxidation Layers, Metals. (Basel) 11 (12) (2021) 2061.
[39] L. Monaco, R.N. Sodhi, G. Palumbo, U. Erb, XPS study on the passivity of coarse-grained polycrystalline and electrodeposited nanocrystalline nickel-iron (NiFe) alloys, Corros. Sci. 176 (2020) 108902.
[40] M. Li, K. Yang, M. Zhang, Y. Liu, L. Ding, J. Teng, G. Yu, XPS analyses on Ta/Au/NiFe/NiO/Ta films, Surface Interface Anal. 47 (4) (2015) 540–544.
[41] B. Panigrahi, S.K. Sahoo, S. Syamlal, J. Sinha, H. Basumatary, M.M. Raja, A. Haldar, Effect of Ta capping layer on spin dynamics in Co50Fe50 thin films, Solid. State Commun. 348 (2022) 114743.
[42] M. Khanuja, H. Sharma, B. Mehta, S. Shivaprasad, XPS depth-profile of the suboxide distribution at the native oxide/Ta interface, J. Electron. Spectros. Relat. Phenomena 169 (1) (2009) 41–45.
[43] X. Wang, Y. Tuo, Y. Zhou, D. Wang, S. Wang, J. Zhang, Ta-doping triggered electronic structural engineering and strain effect in NiFe LDH for enhanced water oxidation, Chem. Eng. J. 403 (2021) 126297.
[44] I. Mihai Miron, G. Gaudin, S. Auffret, B. Rodmacq, A. Schuhl, S. Pizzini, J. Vogel, P. Gambardella, Current-driven spin torque induced by the Rashba effect in a ferromagnetic metal layer, Nat. Mater. 9 (3) (2010) 230–234.
[45] A. Sahoo, A. Mukhopadhyaya, S.P. Mahanta, M.E. Ali, S. Bedanta, Molecular-hybridization-induced antidamping and sizeable enhanced spin-to-charge conversion in Co 20 Fe 60 B 20/β-W/C 60 heterostructures, Phys. Rev. Appl. 21 (5) (2024) 054001.
[46] T. Tanaka, H. Kontani, M. Naito, T. Naito, D.S. Hirashima, K. Yamada, J.-i. Inoue, Intrinsic spin Hall effect and orbital Hall effect in 4 d and 5 d transition metals, Phys. Rev. B 77 (16) (2008) 165117.
[47] I. Oh, J. Park, D. Choe, J. Jo, H. Jeong, M.-J. Jin, Y. Jo, J. Suh, B.-C. Min, J.-W. Yoo, A scalable molecule-based magnetic thin film for spin-thermoelectric energy conversion, Nat. Commun. 12 (1) (2021) 1057.